Biometric Recognition via Eye Movements: Saccadic Vigor and Acceleration Cues

IOANNIS RIGAS and OLEG KOMOGORTSEV, Texas State University
REZA SHADMEHR, Johns Hopkins University

Previous research shows that human eye movements can serve as a valuable source of information about the structural elements of the oculomotor system and they also can open a window to the neural functions and cognitive mechanisms related to visual attention and perception. The research field of eye movement-driven biometrics explores the extraction of individual-specific characteristics from eye movements and their employment for recognition purposes. In this work, we present a study for the incorporation of dynamic saccadic features into a model of eye movement-driven biometrics. We show that when these features are added to our previous biometric framework and tested on a large database of 322 subjects, the biometric accuracy presents a relative improvement in the range of 31.6–33.5% for the verification scenario, and in range of 22.3–53.1% for the identification scenario. More importantly, this improvement is demonstrated for different types of visual stimulus (random dot, text, video), indicating the enhanced robustness offered by the incorporation of saccadic vigor and acceleration cues.

Categories and Subject Descriptors: H.1.2 [**Models and Principles**]: User/Machine Systems—*Human information processing*; I.5.1 [**Pattern Recognition**]: Models—*Statistical*

General Terms: Human Factors

Additional Key Words and Phrases: Eye movement biometrics, saccadic vigor, saccadic acceleration

ACM Reference Format:

Ioannis Rigas, Oleg Komogortsev, and Reza Shadmehr. 2016. Biometric recognition via eye movements: Saccadic vigor and acceleration cues. ACM Trans. Appl. Percept. 13, 2, Article 6 (January 2016), 21 pages.
DOI: http://dx.doi.org/10.1145/2842614

1. INTRODUCTION

Human eye movements serve as a vital mechanism for the selection of information from the visual environment. The physical structure of the oculomotor system is formed by the eye globe; six extraocular muscles working in agonist–antagonist pairs; and various surrounding tissues, liquids, and ligaments. Of the six extraocular muscles, the lateral and medial recti are responsible for horizontal eye movements, the superior and inferior recti are responsible for vertical eye movements, and the superior and

This work is supported in part by the NSF CAREER Grant #CNS-1250718 and the NIST Grant #60NANB14D274. Special gratitude is expressed to Dr. Evgeny Abdulin, T. Miller, Ch. Heinich, and N. Myers for proctoring eye movement recordings.
Authors' addresses: I. Rigas, Texas State University, Department of Computer Science, 601 University Drive, San Marcos, Texas 78666; email: rigas@txstate.edu; O. Komogortsev, Texas State University, Department of Computer Science, 601 University Drive, San Marcos, Texas 78666; email: ok11@txstate.edu; R. Shadmehr, Johns Hopkins University, 720 Rutland Ave, 410 Traylor Building, Baltimore, MD 21205-2195; email: shadmehr@jhu.edu.

DOI: http://dx.doi.org/10.1145/2842614

inferior oblique are mainly responsible for torsional eye movements. The movements of the eye are coordinated by sequences of brain-generated pulses transferred via the oculomotor nerve (for the medial, superior, inferior recti, and inferior oblique muscles), the trochlear nerve (for the superior oblique muscle), and the abducens nerve (for the lateral rectus muscle) [Leigh and Zee 2006].

The first systematic studies of eye movements were conducted in the late 19th century and involved the investigation of eye movements during reading [Javal 1878]. These early studies showed that when a person processes a visual stimulus (e.g., text), the eyes do not move in a homogeneous (continuous) manner but make extremely fast movements from one point of focus to another. These fast movements are called *saccades*, and the points of focus are called *fixations*. In the following years, research regarding eye movements during different visual processing tasks progressed further [Buswell 1935; Just and Carpenter 1980; Yarbus 1967]. A specific branch of research investigated the relation between eye movements and perception. The experiments of Eckstein et al. [2007] showed the existence of similarly activated neural mechanisms for perception and oculomotor action during visual search, whereas the work of Collins and Doré-Mazars [2006] investigated the effects of saccadic adaptation in perception. Furthermore, there were various studies exploring the interconnections between eye movements and selective attention [Holcomb et al. 1977; Kowler et al. 1995]. A more detailed review of the research studies related to the eye movements and perception can be found in Schutz et al. [2011]. The research of Noton and Stark [1971a, 1971b] and Choi et al. [2014] showed that, apart from the visual stimulus and the executed task, the eye movement strategies can also be influenced by idiosyncratic characteristics of the subject. The existence of intrasubject similarities in performed eye movement patterns was also reported in the study of Schnitzer and Kowler [2006], where eye movement activity was explored in the case of repeated readings of text.

The findings from these earlier studies can support the research of eye movements as a source of biometric information. Generation of eye movements involves two mechanisms that can produce intersubject differences: (i) the physical oculomotor structure of every person and (ii) the brain activity-supporting functions of vision that can be connected to cognition and perception [Choi et al. 2014]. The newly established research field of eye movement biometrics utilizes the interperson dissimilarities in the execution of eye movements and concentrates on the formation, comparison, and classification of the respective biometric templates. Although the reliability of eye movement biometrics is still not comparable to traditional biometric recognition approaches like iris scanning, utilization of eye movement biometric cues can offer substantial advantages in terms of spoofing resistance [Komogortsev et al. 2015]. The functional components of the oculomotor system (eye globe, extraocular muscles, and brainstem) are well hidden inside the eye cavity, and their manifestation in the form of eye movements is not static and cannot be replicated from a single image, as it can be potentially done for modalities like fingerprints, face, and iris [Marcel et al. 2014]. Eye movements can be captured remotely and in an unobtrusive way along with other biometric modalities from the eye region, such as the iris [Komogortsev et al. 2012b]. Thus, they provide an appealing natural interface for the extraction of biometric information during interactions with future wearable devices (e.g., Google Glass [Google]). Finally, because eye movements are a product of the human visual system that engages a variety of brain regions, manifestation of pathologies occurring in those regions can be detected in the features extracted from eye movements. An example involves the use of eye movements for the detection of mild traumatic brain injuries [Cifu et al. 2015; Komogortsev and Holland 2014]. In particular, Shadmehr et al. [2010] has suggested that the speed with which the eyes move during a saccade (i.e., saccade vigor) may be a reflection of between-subject differences in patterns of decision-making in health and disease. Also, eye movements can be used to evaluate a user's fatigue [Abdulin and Komogortsev 2015; Yingying et al. 2014]. In this context, the extraction of biometric features from eye

movements provides a unique opportunity for the creation of "smart biometric systems" that combine recognition and health monitoring using the same hardware and software.

1.1 Prior Art

The initial potential of eye movement biometrics was demonstrated in the work of Kasprowski and Ober [2004]. The analysis of eye movement characteristics using the Cepstrum transform brought about a False Acceptance Rate[1] (FAR) of 1.36% and a False Rejection Rate[1] (FRR) of 12.59% for a small test database of nine persons. Subsequent studies were based on a similar rationale and applied signal processing techniques already used in other domains. In the work of Bednarik et al. [2005], properties of eye movement signals were inspected by applying the Fast Fourier Transform (FFT) and Principal Component Analysis (PCA). The best result for dynamic eye movement features using a database of 12 persons was a classification rate (correct identification) of 56%. In the work of Kinnunen et al. [2010], techniques from the field of voice recognition were applied to eye movement signals to achieve an Equal Error Rate[1] (EER) of 30% using a database of 17 persons.

The work presented in Komogortsev et al. [2012a] proposed a methodology based on the use of a model of the oculomotor system for the simulation of eye saccades. By comparing simulated eye movements with real ones, a set of modeling features was extracted and then used for biometric verification of human subjects. The achieved Half Total Error Rate (i.e., the average of FAR and FRR) for 59 subjects was 19%. The method was further modified in Komogortsev et al. [2014b] and tested both on a high-resolution database (32 subjects) and a low-resolution database (172 subjects). The achieved EER for the first database was 20.3% and the Rank-1 Identification Rate[1] (Rank-1 IR) was 65.7%, whereas for the second database the EER was 22.2% and the Rank-1 IR was 12.6%.

Another category of techniques examined the spatial distribution of eye movements with respect to visual stimulus. A characteristic example of this category is the graph-based technique presented in Rigas et al. [2012a]. In this case, the multivariate Wald-Wolfowitz runs test was used for the comparison of spatial distributions of fixation points. The achieved EER for a dataset of 15 subjects was 30%, and the identification rate was 70%. In the work of Cantoni et al. [2015], a gaze analysis technique (GANT) based on graph modeling was tested for a larger population of 112 subjects, achieving a Rank-1 IR of 31.25% and an EER of 22.4%. An alternative spatial representation was proposed in Rigas and Komogortsev [2014] with the use of a set of probabilistic activation maps (fixation density maps-FDM) for the representation of fixation point distributions during the observation of video sequences. The achieved performances for single enrollments and for a large database recorded from 200 subjects were a top Rank-1 IR of 32.8% and a minimal EER of 12.1%.

A large number of methods investigated the extraction and employment of features describing the properties of fixation and saccadic profiles. In the work of Rigas et al. [2012b], the graph-based scheme previously used in Rigas et al. [2012a] was employed to compare velocity and acceleration features extracted from fixation profiles. The method achieved a Rank-1 IR of 82% for a database of 79 subjects and 91.5% for a smaller database of 37 subjects. In the work presented by Holland and Komogortsev [2013a], different characteristics from fixations and saccades were modeled using a Gaussian CDF and combined using a weighted fusion scheme. Databases with different numbers of subjects were used (22, 32, 173 subjects), with the best EER being 28% and the best Rank-1 IR being 53% (for the database of 32 subjects). The method was improved in the Complex Eye Movement Behavior (CEM-B) framework presented in Holland and Komogortsev [2013b], where the distributions of primitive characteristics of fixations and saccades related to duration, amplitude, and velocity were compared using different statistical tests (Ansari-Bradley, Mann-Whitney U-test, Kolmogorov-Smirnov, and Cramér-von Mises).

[1]For definitions of performance metrics see Section 4.1.

The performance for a database of 32 subjects was a minimal EER of 16.5% and a Rank-1 IR of 82.6%. In the work presented by Zhang and Juhola [2012], data mining techniques (Neural Networks, SVM, RBF) were applied on saccadic features (amplitude, accuracy, latency, velocity, and acceleration) and reported a verification rate of about 90% for a database of 132 subjects. Also, the study of Yoon et al. [2014] used Hidden Markov Models (HMM) to model the relationships between gaze velocities in the case of cognitive visual stimulus composed of dot patterns. The classification performance for a small pool of 12 subjects ranged between 53% and 76%.

1.2 Motivation and Contribution

In this work, we present a comprehensive investigation of the effects obtained from integrating dynamic cues modeling of the saccadic properties into the CEM-B framework [Holland and Komogortsev 2013b]. The proposed scheme is based on the representation of saccadic vigor as an expression of the peak velocity and amplitude relationship [Choi et al. 2014] and on the modeling of saccadic acceleration and deceleration characteristics. The selected baseline biometric framework (CEM-B) in which the new features are integrated has already shown its efficacy for simpler features such as the duration, amplitude, and velocity of eye movements. We hypothesize that the incorporation of features that model more complex phenomena encoded in eye movements should improve the overall biometric performance. To test our hypothesis, we perform an extensive evaluation of the effects obtained from the integration of the new dynamic features in terms of recognition accuracy and robustness when using different types of visual stimulus.

The motivation for exploring the biometric potential of saccadic vigor was inspired by the recent work of Choi et al. [2014] that investigated the relationship between saccadic vigor and the impulsivity of subjects in a decision-making task. The results of this study showed the existence of a particular degree of idiosyncrasy in saccadic vigor that was correlated with decision-making behavior (i.e., subjects with higher vigor had a steep temporal discount function during the decision-making task). Also, previous studies have associated the vigor of a saccadic movement with the activity of the "buildup" cells in the intermediate layers of the superior colliculus (SC) [Ikeda and Hikosaka 2007], the primary integrating area for eye movements.

Our work also explores the relationship between the acceleration and deceleration of saccadic eye movements by modeling the characteristics of saccadic acceleration profiles. In the past, the variability of dynamic saccadic features like peak velocity and the magnitude of peak acceleration were explored by Abrams et al. [1989]. The acceleration of a moving body (e.g., the eye globe) reflects the properties of the mechanisms that apply the moving forces; in this case, the muscles and neural pulse signals. The work of Carlton and Newell [1988] showed that variability in maximum acceleration can provide indications about the variability of force parameters. Thus, we can hypothesize that the examination of the saccadic acceleration profile can provide information about the possible differences in the viscosity/elasticity of the muscles and/or their control functions.

The contribution of our work in the field of eye movement biometrics can be summarized as follows:

- We employ saccadic vigor as a biometric trait.
- We employ features modeling saccadic acceleration as a biometric trait.
- We evaluate the improvement afforded by saccadic vigor and acceleration over previous baseline.
- We investigate the robustness of the new biometric scheme for different visual stimuli.

2. METHODS

In this section, we describe the theoretical background related to the extraction of saccadic vigor and acceleration features and their incorporation into the CEM-B biometrics framework.

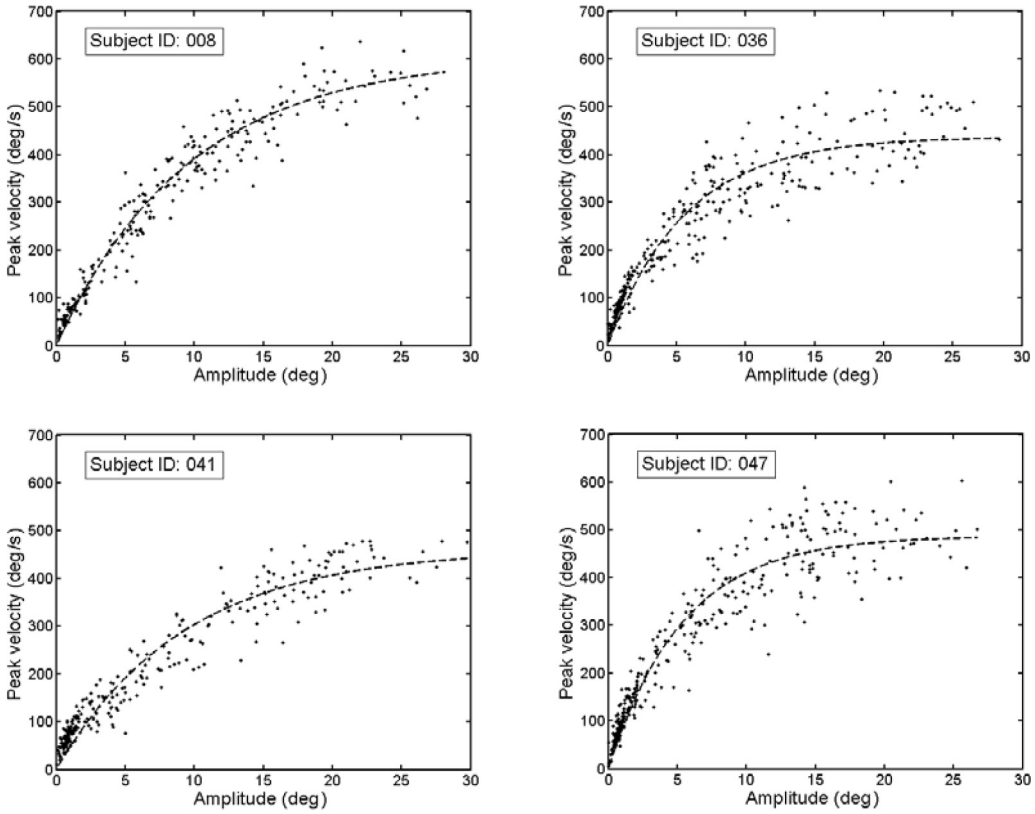

Fig. 1. Representation of the peak velocity–amplitude relationship (main sequence) for saccades recorded from different subjects in our database. In all cases, the figure shows the horizontal component of the eye movement.

2.1 Modeling of Saccadic Vigor Features

The exploration of the relationships governing the basic characteristics of the saccades (e.g., the duration, amplitude, and peak velocity) has been the topic of various studies in the past. The work presented by Bahill et al. [1975] established the term "main sequence" (borrowed from astronomy) to describe the relationships between peak velocity and duration and between peak velocity and amplitude (or magnitude) of saccadic eye movements. It was observed that the peak velocity increases almost linearly with saccadic duration, whereas the relationship between the peak velocity and saccadic amplitude deviates from linearity for saccades of increasing amplitude until it reaches a plateau. These findings were partially supported also by previous studies in the field [Robinson 1964; Zuber et al. 1965]. Despite the generally stereotyped behavior of saccadic characteristics, their exact values can vary due to several reasons. The main sources of variability in the characteristics modeled by the "main sequence" have been researched by a number of works [Abrams et al. 1989; Bahill et al. 1981; Bollen et al. 1993]. Furthermore, the main sequence and the variability of the saccadic characteristics have been explored in more recent studies using video-based eye-trackers [Di Stasi et al. 2011; Haith et al. 2012; van Beers 2007].

In Figure 1, we demonstrate the main sequence diagrams representing the saccades recorded from different subjects of our database. For comparison reasons, all the plots show the peak velocity–amplitude relationship for the horizontal component of the eye movement. In the specific experiment,

the subjects were observing a "random jumping" dot of light, and thus saccades of various amplitudes were acquired. A curve is fitted to the scattered data to exhibit the nonlinear shape of the main sequence. During the processing of the recordings, any saccades with peak velocities $>1{,}000^\circ$/s and amplitudes $>100^\circ$ were filtered out since these values cannot physically represent actual saccades and should be attributed to various recording artifacts (e.g., eye blinks). A first observation of the data verifies the theoretically expected behavior of the main sequence, which deviates from linearity as the saccadic amplitudes get larger. A closer inspection reveals noticeable intersubject variations in the data-fitted shape of the main sequence and also in the exact degree of data scattering (dispersion from the fitted curve).

The work presented recently by Choi et al. [2014] investigated saccadic vigor as an expression of the peak velocity–amplitude relationship in relation to decision-making cost. The findings of this work supported that if we denote the across-subject peak velocity–amplitude function by *g(x)*, then we can approximate the peak velocity of saccade j for subject i as a scaled version of this function:

$$v_i^{(j)} = a_i \cdot g\left(x_i^{(j)}\right). \tag{1}$$

The scaling factor a_i can be employed as a gauge of the vigor of saccades for subject i. The conducted experiments showed that the values of vigor can present an idiosyncratic nature and also that they appear to be closely related to the anticipation behavior of every subject i. Based on these findings, we explored the intersubject variability of saccadic vigor and investigated its potential as a biometric feature. To this purpose, we calculated the vigor of saccades performed by a subject during the observation of visual stimuli. The feature vectors were formed by the distributions of the extracted vigor values and were integrated into the biometric templates. The use of the vigor–value distributions instead of a unique value from the entire recording was opted as a more robust approach for capturing any subject-specific behavior differences during the manifestation of vigor over time.

Saccadic peak velocities can be determined by their respective saccadic velocity profiles. The procedure for the calculation of velocity involves the first-order derivative of the eye movement positional signal. Computing a derivative can emphasize the presence of noise, especially for eye-trackers operating at high frequencies, as was the one used in our experiments. Thus, for the calculation of velocity from the positional signal, we opted to use the smoothing derivative formula proposed by Bahill and McDonald [1983]. Let us denote the raw positional eye movement signal with x and the sampling period with T_s. The formula for calculating the velocity of the *k-th* sample is:

$$v\,(k) = (x\,(k+3) - x\,(k-3))\big/(6 \cdot T_s). \tag{2}$$

Assuming a sampling frequency of 1,000Hz, the achieved cutoff frequency (-3dB) is higher than 75Hz, and the significant information about saccades is not filtered out [Bahill and McDonald 1983].

Using the calculated velocity signal, we can extract velocity profiles for the individual saccades of a recording. First, we need to partition the eye movement recording into sequences of individual fixations and saccades. To this purpose, we employ the velocity threshold classification algorithm (I-VT) described in Salvucci and Goldberg [2000]. The specific algorithm takes as an input the smoothed velocity signal calculated using Equation (2), and, after its parameterization, it classifies all the samples with velocity over a threshold as belonging to a saccade (otherwise they belong to a fixation). During the second step of the algorithm, the samples that are classified as belonging to a saccade (or fixation) are merged to form the profiles of the individual saccades (or fixations) performed by the subject. In our current incarnation of the algorithm, we use a velocity threshold of 30°/s. Also, a "micro-saccadic" filter is applied to reclassify any saccades with an amplitude of $<0.5^\circ$ (micro-saccades), and a "micro-fixation" filter is applied to reclassify any fixations with a duration of <100ms. The values employed for the velocity and post-filtering thresholds are based on the normative values of human

eye movement data [Leigh and Zee 2006]. Because the I-VT algorithm does not restrict the detection only to saccades occurring directly after some specific changes in the visual stimulus, it can also detect spontaneous saccades. However, the specific implementation of the I-VT algorithm cannot detect more complex movements such as smooth pursuits.

The first step for modeling the vigor of individual saccades is to determine a suitable generic nonlinear function for representing the parametric relationship between the peak velocity and amplitude of the saccades. Different empirical functions can be used to fit the data, and, in the current work, we employ the following inverse exponential function proposed by Baloh et al. [1975]:

$$y = a(1 - \exp(-x/b)). \tag{3}$$

In Equation (3), b is a rate parameter. To compute the vigor for each saccade, we follow two steps. Initially, we use a development set with saccades from different subjects (for more information on the development and evaluation sets, see Section 4.1), and, for each subject, we fit Equation (3) to the saccadic data. By averaging the across-subject (development set) rate parameter values—calculated via the curve fitting—we estimate the final value for b_{avg}. Then, we can solve Equation (3) to estimate the vigor of each individual saccade j made by a subject i (evaluation set), as follows:

$$a_i^j = {v^{peak}}_i^j / \left(1 - \exp\left(-amp_i^j / b_{avg}\right)\right). \tag{4}$$

The complete vigor feature vector for an eye movement recording from subject i is formed by using the distribution of the vigor values corresponding to the N saccades extracted from the recording: $f_i^{vig} = \{a_i^1, a_i^2, \ldots, a_i^N\}$.

The use of the vigor features is expected to provide more robustness across different types of visual stimuli (that induce saccades of different amplitudes) than considering the peak velocity and amplitude separately. An alternative option for providing robustness across different stimuli would be to take the ratio of peak velocity and amplitude. However, modeling of the peak velocity–amplitude relationship using a nonlinear formula can provide a more accurate representation, as indicated by previous research studies [Bahill et al. 1975; Robinson 1964; Zuber et al. 1965].

2.2 Modeling of Saccadic Acceleration Features

Saccadic eye movements are executed via the combined application of agonist–antagonist forces from the oculomotor muscles. Thus, inspecting the acceleration profile of a saccade can provide valuable information regarding the underlying sources of the applied forces. During the execution of a saccade, eye velocity initially increases (acceleration phase) until it reaches a maximum value (peak velocity); then, velocity starts decreasing (deceleration phase) until the eye reaches its new position. Although the laws of physics require that the area for the acceleration phase must equal the area for the deceleration phase in the force–time profiles, this does not mean that the two parts of the curve need to mirror each other. For example, the force during the deceleration phase can have a smaller magnitude and be applied for a larger duration [Abrams et al. 1989]. To avoid any confusion in the subsequent description, the term *acceleration profile* refers to the curve containing both the *acceleration phase* (velocity increasing) and the *deceleration phase* (velocity decreasing).

The existence of asymmetries in acceleration profiles has been reported by several studies in the past. In the study of Thomas [1969], the lack of symmetry was observed in the case of vertical saccades of different directions, compared to the more symmetric form of the horizontal saccades of different directions. The different behavior for the vertical and horizontal saccades was attributed by the author to the stiffer elasticity of the horizontal recti muscles compared to the composite stiffness of the four muscles involved in vertical eye rotations. Another important finding of this study was that acceleration profiles coming from different saccades can be similar in their initial parts but subsequently

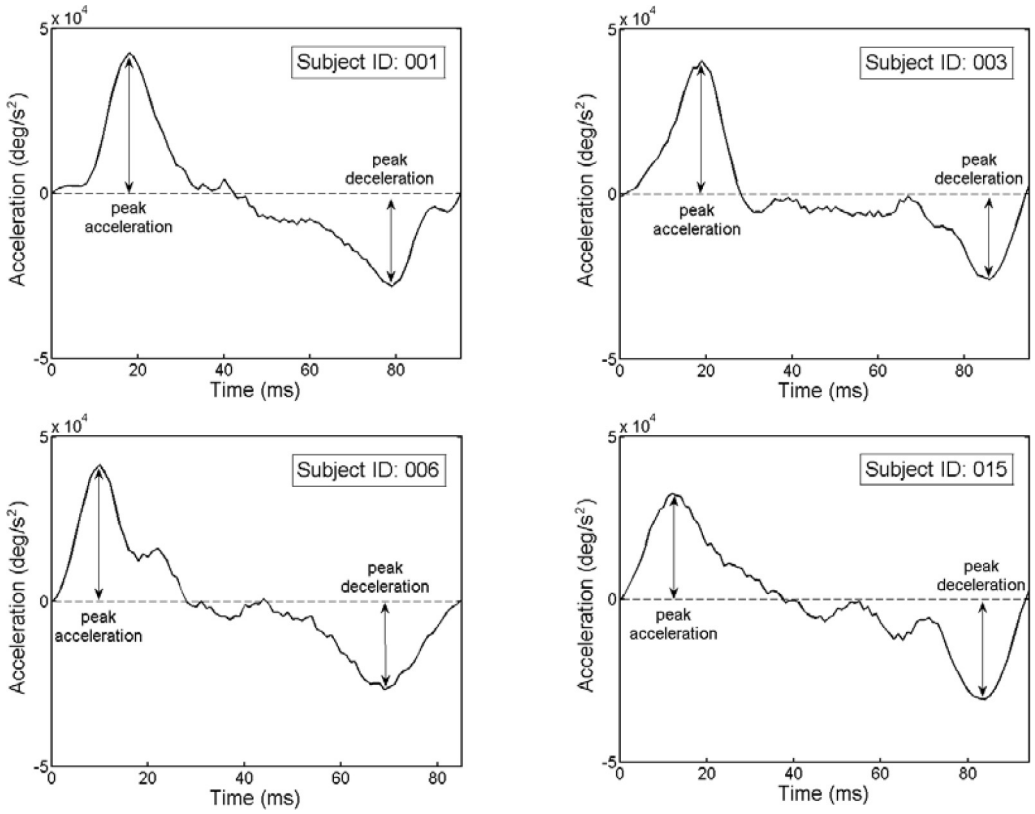

Fig. 2. Presentation of the acceleration profiles for saccades executed by different subjects. Saccades correspond to the same stimulus (point of light) placed to induce horizontal saccades with amplitude of 30° (eye moving from −15° to 15°).

may diverge. In the work of Fricker [1971], it was reported that the acceleration phase and the deceleration phase in the acceleration profiles can exhibit small asymmetries (e.g., the peak deceleration was found to be somewhat smaller than the peak acceleration). The work of Abrams et al. [1989] investigated the dynamic properties of eye movements with a particular focus on the speed–precision tradeoff of saccadic movements. During the inspection of acceleration profiles for saccades of different amplitudes, the peak deceleration appeared slightly smaller in magnitude compared to the peak acceleration, and the deceleration part of the curve was slightly skewed toward the end. Furthermore, the work of Collins et al. [2008] explored the dynamics of saccades during saccadic adaptation, and the findings of this study showed that it is the decelerating phase that tends to be modified by motor learning.

In the current work, we extracted descriptive characteristics from the acceleration profiles of saccades and modeled the asymmetries of the acceleration and deceleration phases. In Figure 2, we present example acceleration profiles for saccades executed by different subjects. The saccades correspond to the same stimulus (i.e., a "jumping" point of light placed to induce horizontal saccades of approximately 30° [eye moving from −15° to 15°]).

An inspection of the acceleration profiles reveals the existence of variations in (a) the overall profile shape, (b) the absolute peak values, and (c) the ratio of the peak acceleration and peak deceleration values. Apart from intersubject differences, there are also variations in the acceleration profiles of

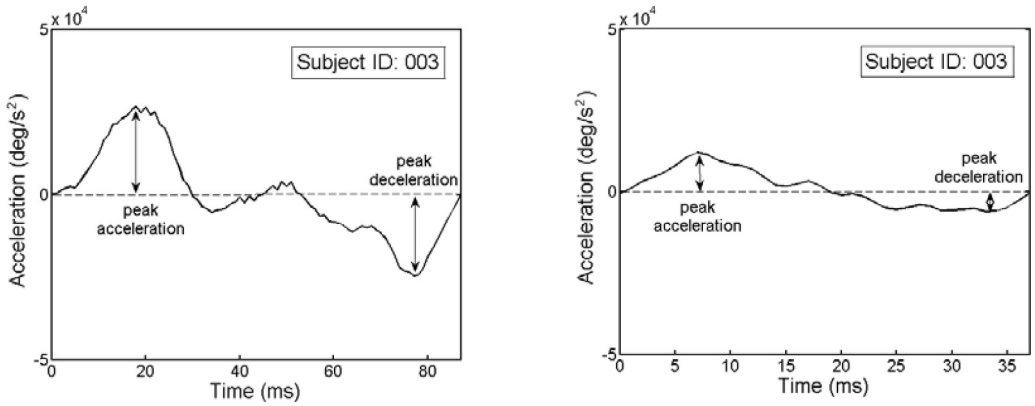

Fig. 3. Presentation of the acceleration profiles for saccades of large and small amplitude executed by the same subject. The first profile (left) corresponds to a saccade of amplitude 20° and the second (right) to a saccade of amplitude 3°.

saccades coming from the same subject. The exact acceleration values depend on the exact amplitudes of the executed saccades. Saccades of larger amplitudes induce larger peak accelerations and decelerations. In Figure 3, we show the acceleration profiles for saccades of large and small amplitude coming from the same subject. The goal of our work is to extract those features that emphasize intersubject variations with minimum interference from intrasubject variations.

The procedure for extracting the acceleration features initiates with the calculation of the second derivative from the positional eye movement signal. As in the case of velocity, we employed the corresponding smoothing second derivative formula suggested by Bahill and McDonald [1983]. For the calculation of acceleration for the raw positional sample k and sampling period of T_s, we have:

$$acc(k) = (vel\,(k+4) - vel\,(k-4))\big/(8 \cdot T_s). \tag{5}$$

Then, based on the extracted saccade boundaries given by the used classification algorithm (I-VT), we can extract the acceleration profiles for the individual saccades. The proposed features for the representation of the characteristics of saccadic acceleration profiles are related both to the overall shape of the profile and to the relative difference (ratio) of peak magnitudes during the acceleration and deceleration phases (accommodating thereby for saccades of different amplitudes). Let us denote ${acc^{prof}}_i^j$ the acceleration profile corresponding to a saccade j made by subject i. The first type of features is extracted by calculating the mean activation m_i^j over the entire saccadic acceleration profile, thus providing an aggregated representation of the means during the acceleration and deceleration phases (i.e., ${m^{acc}}_i^j = \sum_{k=1}^{L} {acc^{prof}}_i^j(k)/L$ and ${m^{dec}}_i^j = \sum_{k=L+1}^{K} {acc^{prof}}_i^j(k)/K - L - 1$), where L are the samples of the acceleration phase and K are the samples representing the whole acceleration profile.

The second type of acceleration features model the relative differences between peak accelerations and decelerations. The peak acceleration ratio for a saccade j made by subject i is calculated as follows:

$$r_i^j = \left|\max_k \left({acc^{prof}}_i^j\right)\right| \Big/ \left|\min_k \left({acc^{prof}}_i^j\right)\right|. \tag{6}$$

The two types of acceleration feature vectors for a recording coming from subject i are formed using the distributions of all the respective values from the extracted N saccades: $f_i^{acc\_m} = \{m_i^1, m_i^2, \ldots, m_i^N\}$ and $f_i^{acc\_r} = \{r_i^1, r_i^2, \ldots, r_i^N\}$.

Table I. Overview of the CEM-B Features and the New Dynamic Features Based on Saccadic Vigor and Acceleration

Original CEM-B features (duration, position, velocity)		New dynamic features (vigor, acceleration)
1. Start time (fixation)	*7. Horizontal amplitude (saccade)*	*13. Horizontal saccadic vigor (saccade)*
2. Duration (fixation)	*8. Vertical amplitude (saccade)*	*14. Vertical saccadic vigor (saccade)*
3. Horizontal centroid (fixation)	*9. Horizontal mean velocity (saccade)*	*15. Horizontal mean acceleration (saccade)*
4. Vertical centroid (fixation)	*10. Vertical mean velocity (saccade)*	*16. Vertical mean acceleration (saccade)*
5. Start time (saccade)	*11. Horizontal peak velocity (saccade)*	*17. Horizontal acceleration ratio (saccade)*
6. Duration (saccade)	*12. Vertical peak velocity (saccade)*	*18. Vertical acceleration ratio (saccade)*

2.3 Incorporation of Features into Complex Eye Movement Behavior Biometrics

During the biometric recognition experiments, the features extracted for vigor f_i^{vig} and acceleration $f_i^{acc\_m}$, $f_i^{acc\_r}$ are integrated into the CEM-B framework [Holland and Komogortsev 2013b]. The employment of the CEM-B framework provides two advantages: (i) the easy integration of the new dynamic features as univariate distributions along with the other features of the framework and (ii) the possibility for a direct evaluation of the achieved improvement from the integration of the new features compared to the baseline performance of the original features. The extracted features are calculated separately for the horizontal and vertical components of the eye movement. This modeling leads to a more robust representation of the characteristics of the underlying muscles and neural pulses, given the existing differences in the oculomotor system, previously reported in Bahill and Stark [1975]. The effects from these differences are also supported by the observed differences in the profiles of the horizontal and vertical saccades [Collewijn et al. 1988a; Collewijn et al. 1988b].

In Table I, we present the original CEM-B features and the new proposed features added to the framework. The original CEM-B algorithm extracts a set of four fixation and eight saccade features related to duration, position, and velocity. With the integration of the new features of saccadic vigor and acceleration, the framework will contain a total of 18 features. These features are treated separately as univariate distributions, and their comparison can be performed with the use of different distribution similarity measures. In the current work, we use the Two-Sample Kolmogorov-Smirnov test as the preferred distribution comparison measure. During our preliminary experiments, we also tested the Two-Sample Cramer-von Mises test but it was found to present equal or inferior performance.

After the comparison phase, we end up with 18 similarity matrices containing the pairwise scores from the compared feature vectors. These matrices will be combined to generate a single similarity score for each pairwise comparison, which will be used to perform the biometric recognition. In this work, we evaluate four fusion schemes for the combination of similarity scores: the Simple Mean—or Sum—(SM) [Snelick et al. 2005], the Weighted Mean based on Rank-1 IR performance (WM) [Rigas et al. 2015], the Random Forests (RF) scheme [Breiman 2001], and the Likelihood Ratio (LR) scheme [Nandakumar et al. 2008]. To train the parameters of the WM, RF, and LR fusion algorithms, we used the development dataset (see Section 4.1). In Figure 4, we provide a schematic diagram summarizing the procedures followed for the extraction of the saccadic vigor and acceleration features and their incorporation into the CEM-B framework for performing the task of biometric recognition.

3. EXPERIMENTS

3.1 Apparatus

The eye-tracking device used was an SR Research EyeLink 1000 eye-tracker [EYELINK], working at 1,000Hz. During the experiments, the measured average calibration accuracy was 0.49° (SD = 0.17°), and the average data validity was 96.8% (SD = 4.9%). The calibration accuracy was calculated via

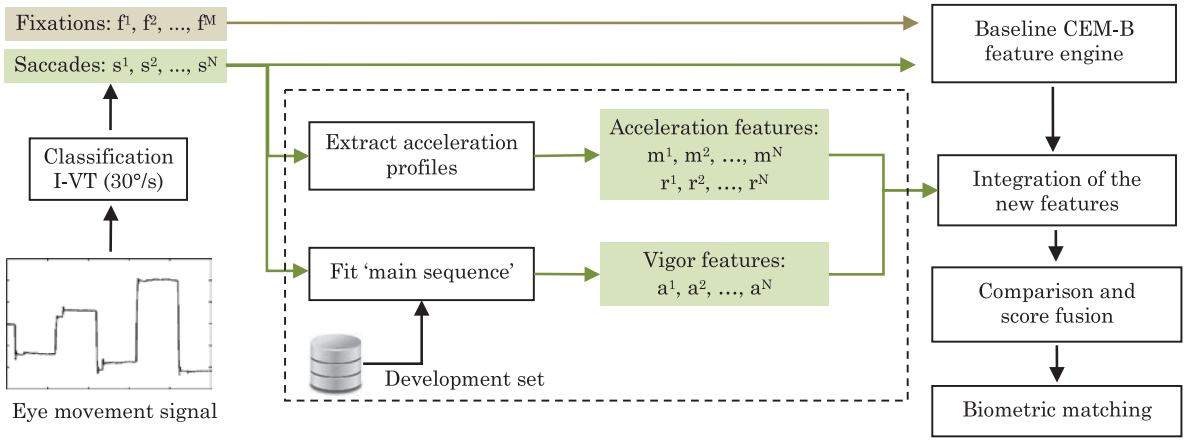

Fig. 4. Diagram of the procedures for the integration of saccadic vigor and acceleration features into the CEM-B framework.

the measurement of the error of the eye landing positions compared to the expected positions of the calibration points (nine points were used in our experiments). The data validity was calculated via the measurement of the total percent of samples that the eye-tracker was not able to capture successfully (e.g., due to blinking, moisture, squinting, etc.). Furthermore, we used artificial eyes provided by SR Research to measure eye-tracking precision (noise), which was found to be 0.034° (SD = 0.006°).

The visual stimuli were presented on a flat-screen monitor with dimensions of 474 × 297mm and resolution of 1680 × 1050 pixels, placed at a distance of 550mm from the subject. To ensure the maximum quality of the recorded data, we used a chinrest with a head bar to stabilize the subject's head.

3.2 Participants

The experiments were conducted with 322 subjects (171 male/151 female), aged 18–46 (M = 22, SD = 4.2). Of those subjects, 163 had corrected vision (67 glasses/96 contact lenses). The subjects performed two recording sessions each, separated by a time interval of approximately 20 minutes for each visual stimulus, leading to the collection of 1,866 unique recordings. Texas State University's institutional review board approved the study, and every subject provided informed consent.

3.3 Visual Stimulus

The visual stimuli were chosen to induce saccades of various amplitudes, peak velocities, and accelerations, thus allowing for the evaluation of the saccadic vigor and acceleration cues. The adopted visual stimuli were the following:

Random "Jumping" Point (RAN): This stimulus consisted of a point (white circle with a black center) appearing at random positions against the black background of a computer screen. The point changed position every 1 second, and the duration of each experimental trial was 1 minute and 40 seconds. The specific stimulus induces random oblique saccades of different amplitudes.

Text Excerpts (TEX): The participants read freely some text excerpts from the poem of Lewis Carroll "The Hunting of the Snark." The total time that was given to the participants to read the excerpts was 1 minute. For the specific stimulus, the amplitudes of the saccades are not totally random, but they can form patterns according to the reading behaviors of the subjects.

Video Sequence (VID): The participants watched freely a part from a video trailer of the Hollywood movie *The Hobbit: The Desolation of Smaug*. The total duration of the video sequence was 1 minute.

For the specific stimulus, the subjects performed more complex patterns of fixations and saccades (and occasionally smooth pursuits) as they observed the dynamically changing video content.

Recordings for RAN, TEX, and VID stimuli were a part of a larger experiment in which subjects performed various eye movement tasks with several periods of rest to reduce possible fatigue effects. Total duration of all tasks and periods of rest did not exceed 1 hour.

4. RESULTS

4.1 Evaluation Procedure

In our experiments we split the data into development and evaluation datasets using 20 random partitions with a subject ratio of 50%–50% (the subjects of the development and evaluation sets did not overlap to avoid any overfitting effects). In each case, the data from the development set were used to train the algorithms' parameters (see Section 2.1 and Section 2.3), and the data from the evaluation set were used for the calculation of the performance rates presented later. All reported rates were calculated by averaging the results over the 20 partitions.

For the evaluation of biometric verification and identification performance we use the following measures:

Equal Error Rate (EER): The EER is a measure of the verification performance of a biometric system. A genuine score is defined as the score from the comparison of biometric samples from the same identity. An impostor score is defined as the score from the comparison of biometric samples from different identities. By defining an acceptance threshold (η) we can compute the False Rejection Rate (FRR) as the percentage of the genuine scores that fall under the threshold η, and the False Acceptance Rate (FAR) as the percentage of the impostor scores that are over η. The True Positive Rate (TPR) can be defined as the percentage of genuine scores that are over the threshold η, and it represents TPR $=$ $1 -$ FRR. By changing the acceptance threshold, we can construct a Receiver Operating Characteristic (ROC) curve and calculate the EER as the point of operation where the FRR equals the FAR. For the construction of the ROC curves, we employed the technique of vertical averaging [Fawcett 2006] over the 20 partitions.

Rank-1 Identification Rate (Rank-1 IR): The Rank-k Identification Rate (Rank-k IR) is a measure of the biometric identification performance that shows the percentage of genuine scores that can be found within the k top places of a ranked list. A Cumulative Match Characteristic (CMC) curve shows the change of the identification rate as a function of the used rank k. The Rank-1 IR is defined as the percent of biometric samples with a correct match in the first place of the ranked list.

4.2 Biometric Recognition Performance

In this section, we evaluate the biometric performance that can be achieved from the integration of the saccadic vigor and acceleration features in the original CEM-B framework. For these experiments, we use the Simple Mean (SM) as a common scheme for fusion in all tested cases. In Section 4.3, we additionally show the performances that can be achieved when using the other fusion schemes (WM, RF, LR). In Figures 5 and 6, we present the achieved EER and Rank-1 IR performances for each type of visual stimulus in the form of bar diagrams, with error bars showing the error margins at a 95% confidence interval. For a comprehensive presentation of the relative improvement offered by the vigor and acceleration features, we show the results in the following four cases: (i) C1: the baseline performance of the original CEM-B framework; (ii) C2: the improvement offered by the incorporation of the vigor features alone; (iii) C3: the improvement offered by the incorporation of acceleration features alone; and (iv) C4: the finally achieved improvement by the incorporation of both types of features. It

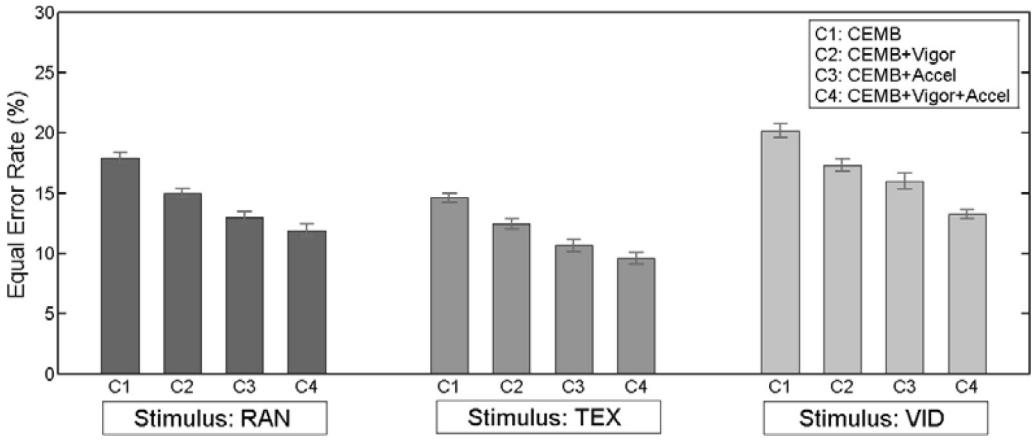

Fig. 5. The EER performances for the different types of visual stimulus.

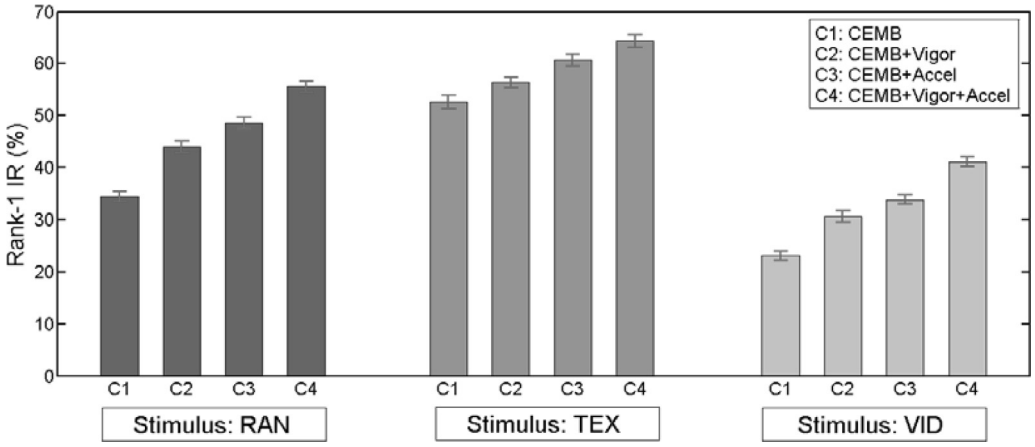

Fig. 6. The Rank-1 IR performances for the different types of visual stimulus.

should be emphasized that during our experiments we used exactly the same settings (comparison/fusion scheme, etc.) for the four cases to ensure a fair comparison.

In the *verification scenario* for the *RAN stimulus* (Figure 5, left) the baseline EER (C1) is 17.92%. The incorporation of the vigor (C2) and acceleration (C3) features separately improves the EER to 14.97% and 13%, respectively. The integration of both types of features (C4) leads to the final EER of 11.92%. For evaluating the significance of the improvements, we performed pairwise one-way ANOVAs across the four cases in the order of successive improvement, using the values from the 20 random partitions. The differences in performance were found to be statistically significant in all cases. For the pair C1–C2 we had $F_{(1,\,38)} = 92.61$, $p < 0.001$, for the pair C2–C3 $F_{(1,\,38)} = 42.18$, $p < 0.001$; and for the pair C3–C4 $F_{(1,\,38)} = 9.63$, $p < 0.01$. In the *identification scenario* for the *RAN stimulus* (Figure 6, left), the baseline Rank-1 IR (C1) is 34.41%, and, with the incorporation of the vigor features (C2), it improves to 44.02%, whereas with the incorporation of the acceleration features (C3), it improves to 48.59%. The integration of both types of features (C4) leads to the final Rank-1 IR of 55.56%. The pairwise one-way ANOVAs reveal that the differences are statistically significant in all cases, and specifically, for the

pair C1–C2 $F_{(1, 38)} = 166.44$, $p < 0.001$, for the pair C2–C3 $F_{(1, 38)} = 34.9$, $p < 0.001$, and for the pair C3–C4 $F_{(1, 38)} = 86.32$, $p < 0.001$.

In the *verification scenario* for the *TEX stimulus* (Figure 5, middle), the baseline value for the EER (C1) is 14.61%. The incorporation of the vigor (C2) and acceleration (C3) features separately improves the EER to 12.45% and 10.64%, respectively. Finally, the integration of both features (C4) improves the EER to 9.57%. The pairwise one-way ANOVAs reveal a significant main effect for the pair C1–C2 with $F_{(1, 38)} = 61.74$, $p < 0.001$, for the pair C2–C3 with $F_{(1, 38)} = 28.45$, $p < 0.001$, and for the pair C3–C4 with $F_{(1, 38)} = 9.03$, $p < 0.01$. In the case of the *identification scenario* for the TEX stimulus (Figure 6, middle), the baseline Rank-1 IR (C1) is 52.58%. With the incorporation of the vigor features (C2), the Rank-1 IR improves to 56.34%, and, with the incorporation of the acceleration features (C3), it improves to 60.65%. The final value of Rank-1 IR after the integration of both features (C4) is 64.29%. The pairwise one-way ANOVAs reveal that all the differences are statistically significant, with the respective values for the pair C1–C2 $F_{(1, 38)} = 21.39$, $p < 0.001$, for the pair C2–C3 $F_{(1, 38)} = 29.01$, $p < 0.001$, and for the pair C3–C4 $F_{(1, 38)} = 18.26$, $p < 0.001$.

In the *verification scenario* for the *VID stimulus* (Figure 5, right), the EER of the baseline CEM-B (C1) is 20.17%. The incorporation of the vigor features (C2) improves EER to 17.30%, and the incorporation of the acceleration features (C3) improves EER to 15.99%. The joint integration of the vigor and acceleration features (C4) leads to the final EER of 13.23%. The pairwise one-way ANOVAs across the 20 random partitions showed a statistically significant difference in all the tested cases. For the pair C1–C2 we had $F_{(1, 38)} = 52.42$, $p < 0.001$, for the pair C2–C3 $F_{(1, 38)} = 9.43$, $p < 0.01$, and for the pair C3–C4 $F_{(1, 38)} = 48.21$, $p < 0.01$. In the *identification scenario* for the *VID stimulus* (Figure 6, right), the baseline Rank-1 IR (C1) has a value of 23.07%. With the incorporation of the vigor features (C2), the Rank-1 IR increases to 30.63%, and, with the incorporation of the acceleration features (C3), it improves to 33.87%. The integration of both types of features (C4) leads to the final Rank-1 IR of 41.10%. The pairwise one-way ANOVAs demonstrate the statistical significance of the reported differences for the pair C1–C2 $F_{(1, 38)} = 106.95$, $p < 0.001$, for the pair C2–C3 $F_{(1, 38)} = 19.48$, $p < 0.001$, and for the pair C3–C4 $F_{(1, 38)} = 111.3$, $p < 0.001$.

The EER and the Rank-1 IR are compact measures that can summarize the verification and identification performance of a biometric recognition system. We also present the ROC and CMC curves to provide a more global overview of the variation of biometric recognition rates when changing the sensitivity of the system. In Figure 7, we show the ROC curve clusters for the four evaluated cases (C1–C4) and for each type of visual stimulus separately. Similarly, in Figure 8, we present the CMC curve clusters for the respective cases. The diagrams allow for a generalized assessment of the relative improvement of the baseline scheme (C1) both when we integrate vigor or acceleration features separately (C2, C3), and when we integrate both feature types (C4).

4.3 Analysis of the Fusion Schemes

In this section, we provide a comparative presentation of the achieved biometric performances when employing different schemes for performing fusion in the comparison score level. In Tables II, III, and IV, we present the calculated values for the EER and Rank-1 IR for the RAN, TEX, and VID stimuli, respectively. An overview of the achieved rates reveals moderate performance differentiations of the employed fusion schemes. The Weighted Mean (WM) fusion scheme provides the optimum overall rates; however, the other schemes can also achieve competitive rates on several occasions. To examine the statistical significance of these differences, we report here the results of the performed ANOVA analyses across selected fusion schemes using the data from the 20 random partitions. In these analyses, we examine only the final case (C4; i.e., after the integration of both vigor and acceleration features) since it yields the finally achieved best recognition rates.

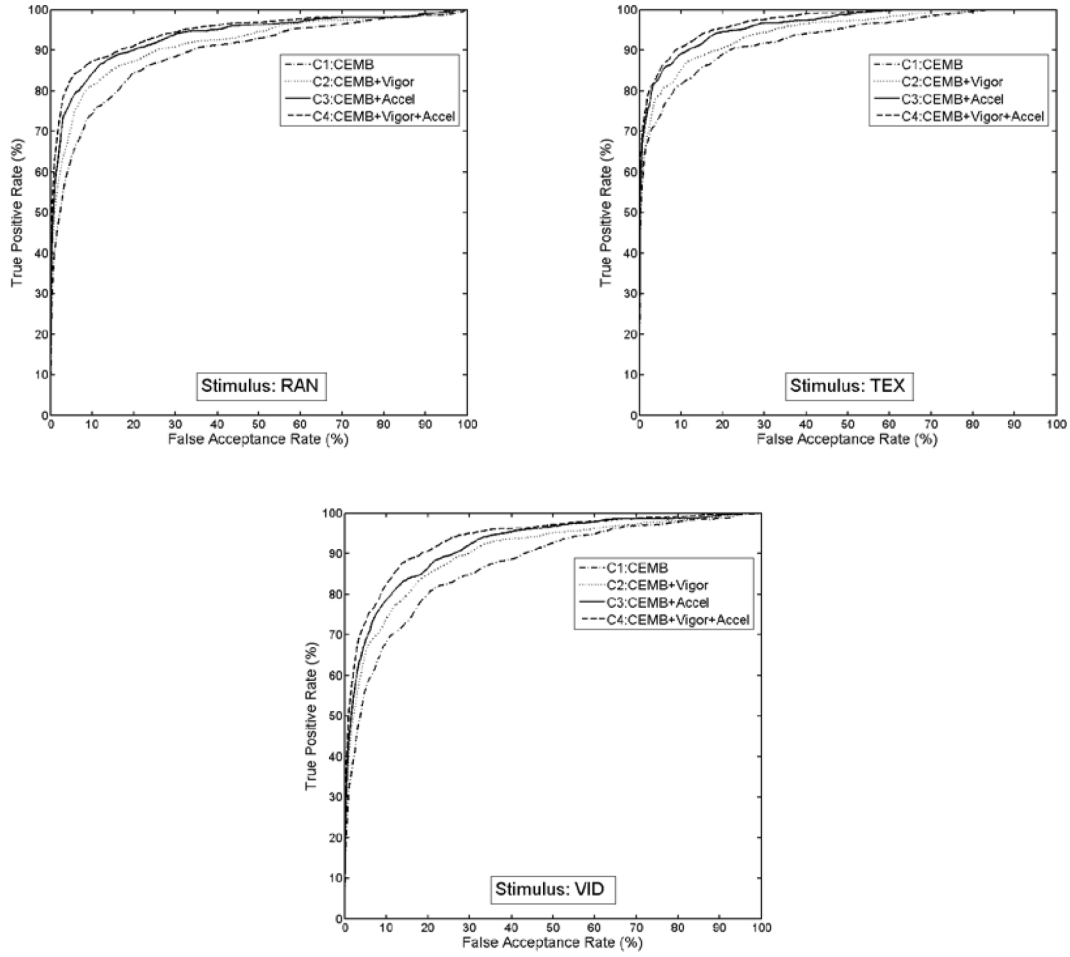

Fig. 7. The constructed ROC curves demonstrating the overall performance in the verification scenario for the different types of visual stimulus.

An inspection of the fusion scheme comparison results for the RAN stimulus (Table II) reveals that, in this case, three of the fusion schemes (SM, WM, LR) yield similar performances, whereas the RF fusion scheme performs worse than the others. In this case, the one-way ANOVA across all schemes reveals a statistically significant main effect, $F_{(3,\,76)} = 23.46, p < 0.001$. The exclusive comparison of the top two performing schemes (WM, LR), though, does not reveal a strong effect, $F_{(1,\,38)} = 3.18, p = 0.08$. For the case of Rank-1 IR, the difference is statistically significant both across all schemes $F_{(3,\,76)} = 54.4, p < 0.001$ and between the top two performing schemes (WM, SM) $F_{(1,\,38)} = 14.79, p < 0.001$.

The fusion scheme comparison results for the TEX stimulus (Table III) reveal again a moderate superiority of the WM scheme over the others. This difference in performance is found to be statistically significant both across all fusion schemes, $F_{(3,\,76)} = 10.46, p < 0.001$ and during the exclusive comparison of the top two performing schemes (WM, RF) $F_{(1,\,38)} = 9.11, p < 0.01$. For the case of Rank-1 IR, the relatively lower performance of the LR scheme induces a significant main effect across all schemes $F_{(3,\,76)} = 67.55, p < 0.001$; however, the comparison of the top two performing schemes (WM, RF) does not show a strong statistical difference $F_{(1,\,38)} = 3.12, p = 0.08$.

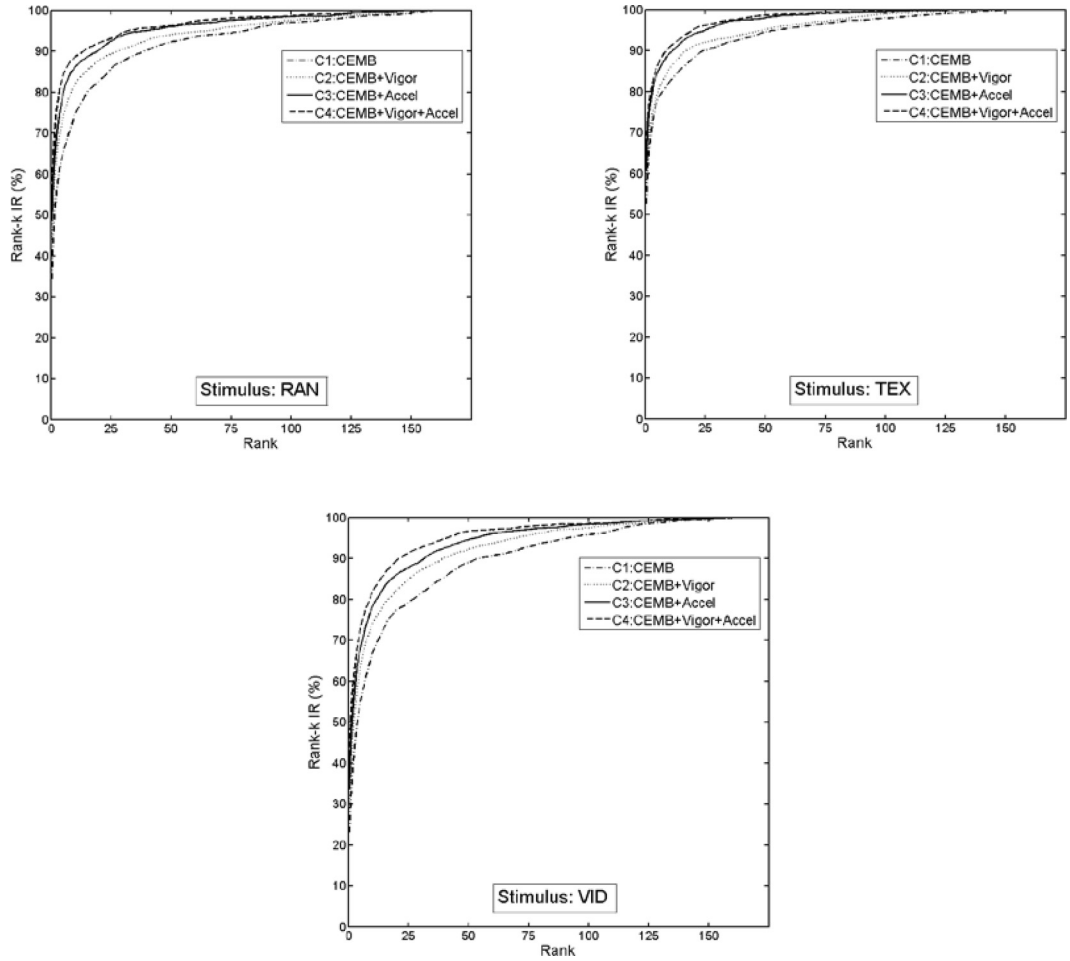

Fig. 8. The constructed CMC curves demonstrating the overall performance in the identification scenario for the different types of visual stimulus.

Table II. Comparison of the Different Fusion Schemes for the RAN Stimulus

Stimulus: RAN								
	EER (SD) %				Rank-1 IR (SD) %			
Case	*SM*	*WM*	*RF*	*LR*	*SM*	*WM*	*RF*	*LR*
C1	17.92 (1.01)	16.46 (0.99)	20.20 (1.09)	16.83 (1.02)	34.41 (2.25)	38.21 (1.94)	29.75 (2.51)	34.58 (2.19)
C2	14.70 (0.92)	13.26 (1.01)	15.81 (1.13)	13.89 (0.98)	44.02 (2.46)	48.93 (2.55)	41.97 (3.44)	46.01 (2.24)
C3	13.00 (0.99)	12.11 (1.24)	15.83 (0.89)	12.68 (0.98)	48.59 (2.43)	51.51 (2.69)	39.97 (2.28)	45.87 (2.01)
C4	11.91 (1.20)	10.95 (1.02)	13.71 (1.03)	11.55 (1.13)	55.56 (2.31)	58.49 (2.51)	47.89 (3.20)	54.11 (2.74)

The biometric performance rates for the VID stimulus presented in Table IV show that, in this case, the effects of the different fusion schemes are even less pronounced. The results of the one-way ANOVA for the EER show a significant main effect across all fusion schemes $F_{(3, 76)} = 51.63$, $p < 0.001$; however, there is no significant main effect across the top two performing schemes (WM, LR) $F_{(1, 38)} = 0.01$, $p = 0.93$. The same results hold for the case of the Rank-1 IR, where the across fusion scheme effect was

Table III. Comparison of the Different Fusion Schemes for the TEX Stimulus

Stimulus: TEX								
	EER (SD) %				Rank-1 IR (SD) %			
Case	*SM*	*WM*	*RF*	*LR*	*SM*	*WM*	*RF*	*LR*
C1	14.61 (0.84)	11.87 (0.80)	12.72 (1.08)	13.08 (0.84)	52.58 (2.74)	54.46 (2.64)	53.88 (3.40)	44.77 (2.75)
C2	12.45 (0.90)	9.51 (0.85)	9.90 (0.84)	10.06 (0.91)	56.34 (2.38)	60.40 (2.49)	60.11 (3.47)	47.81 (3.16)
C3	10.64 (1.21)	8.62 (0.89)	10.69 (1.17)	10.89 (0.69)	60.65 (2.68)	63.52 (2.60)	60.34 (3.09)	52.78 (2.90)
C4	9.57 (1.04)	8.12 (0.86)	8.88 (0.72)	9.13 (0.68)	64.29 (2.70)	66.63 (3.03)	64.69 (3.87)	53.80 (2.87)

Table IV. Comparison of the Different Fusion Schemes for the VID Stimulus

Stimulus: VID								
	EER (SD) %				Rank-1 IR (SD) %			
Case	*SM*	*WM*	*RF*	*LR*	*SM*	*WM*	*RF*	*LR*
C1	20.17 (1.36)	19.39 (1.33)	22.95 (1.58)	18.82 (1.34)	23.07 (2.05)	27.70 (2.99)	27.11 (1.97)	21.43 (1.58)
C2	17.30 (1.14)	14.67 (1.24)	18.63 (1.04)	15.01 (1.52)	30.64 (2.55)	34.57 (2.30)	32.76 (2.48)	28.39 (2.17)
C3	15.99 (1.53)	15.14 (1.40)	18.82 (1.30)	14.65 (1.27)	33.87 (2.06)	37.64 (1.94)	37.24 (1.98)	28.21 (3.11)
C4	13.23 (0.91)	13.13 (0.92)	17.05 (1.57)	13.17 (1.30)	41.10 (2.28)	41.55 (2.64)	40.20 (2.31)	31.91 (3.22)

significant $F_{(3, 76)} = 59.65$, $p < 0.001$, but the top two performing schemes (WM, SM) did not show a significant difference $F_{(1, 38)} = 0.33$, $p = 0.57$.

5. DISCUSSION

5.1 The Effects on Performance

Our main goal was to investigate the extent of improvement that can be achieved by incorporating information about saccadic vigor and acceleration in an eye movement biometric framework. We found that the addition of these features can improve biometric accuracy considerably. The complete extent of the achieved improvement can be quantified in terms of the relative improvement of the final performance (C4) compared to the baseline case (C1). For the case of the verification scenario (EER), the performance for the RAN stimulus improved by 33.5%, the performance for the TEX stimulus improved by 31.6%, and the performance for the VID stimulus improved by 32.3%. For the identification scenario, the relative improvement of Rank-1 IR was even more pronounced: performance improved by 53.1% for the RAN stimulus, by 22.3% for the TEX stimulus, and by 50% for the VID stimulus. Therefore, these results suggest that the addition of vigor and acceleration features can yield a considerable advance both for the baseline performance of the original CEM-B framework and for the field of eye movement biometrics in general.

The improvement in performance was also notable when incorporating each of the proposed features (vigor, acceleration) separately. Specifically, incorporating the vigor features (C2) alone brought about a relative decrease in the EER rates by 19.4% (RAN), 19.9% (TEX), and 24.3% (VID), and a relative increase in Rank-1 IR rates by 28% (RAN), 10.9% (TEX), and 24.8% (VID). Analogously, when incorporating only the acceleration features (C3), there was a relative decrease in the EER rates by 26.4% (RAN), 27.4% (TEX), and 21.6% (VID), and an increase in the Rank-1 IR rates by 34.8% (RAN), 16.6% (TEX), and 35.9% (VID). These results underline the relevance of each of the newly proposed features (vigor, acceleration), and, more importantly, they show that the performance of one feature-type does not negate the performance of another during their common integration into the baseline biometric framework.

During our analysis, we also experimented with different fusion schemes for the combination of information coming from the different features. The evaluated schemes performed with similar rates, with the WM scheme showing the best performance and the most stable behavior. The other schemes interchanged their roles in the second place for the three types of visual stimulus. Furthermore, the VID stimulus seems to be less affected by the selection of a specific fusion scheme. Given the obtained results and considering the increased computational complexity of the more sophisticated fusion schemes (RF, LR), the WM scheme (or alternatively the SM scheme) appears to be the preferred choice for the biometric recognition scenario.

5.2 The Effects of Different Visual Stimuli

One objective of our research was to specifically inspect the impact in performance of the newly proposed features when using different types of visual stimulus. The results revealed that the relative improvement in performance was more emphasized for the cases of the RAN and VID stimuli, whereas the relative improvement for the TEX stimulus was, in most cases, the least among the three types. This result partially confirms our hypothesis that the proposed features can provide a more sophisticated modeling of the relationships between the amplitude, peak velocity, and acceleration of saccades. For example, in the case of the RAN and VID stimuli, the variety in the generated saccadic amplitudes is larger and can therefore justify the greater improvement in performance (almost doubling for Rank-1 IR). In the case of the TEX stimulus, the variety of the saccadic amplitudes can be limited due to the reading pattern layout. It should be noted that the relatively smaller improvement for the TEX stimulus can be also partially attributed to the fact that the performances for the other two types of stimulus start from a worse baseline, thus leaving a larger margin for improvement.

5.3 Practical Applicability Considerations

During the implementation of the experimental recordings, we employed a high-grade eye-tracking device, and we stabilized the subjects' heads in order to ensure the highest possible data quality. It should be noted, though, that during a practical (out-of-the-lab) implementation of a biometric recognition system, several factors can interfere with the capturing procedure, such as unconstrained (free) head movements, variable lighting conditions (inducing variability in the pupil size), and environmental noise. The advances in eye-tracking technology in recent years move toward the mitigation of such effects (e.g., via the development of robust remote and wearable solutions [SMI 2015; THEEYETRIBE 2015; TOBII 2015]) that can perform eye-tracking with acceptable quality in less than ideal conditions. Furthermore, previous research [Holland and Komogortsev 2013a] has shown that the performance loss for eye movement-driven biometrics remains at acceptable levels for specifications of a minimum sampling rate of 250Hz, eye-tracking precision better (lower) than 0.5°, and maximum allowed calibration error lower than 1.5°.

Eye movements require a prolonged recording time compared to static biometric features like the iris and fingerprints. This inherent limitation of eye movements can be counterbalanced by their intrinsic counterfeit resistance properties and also by the given opportunity to build applications for the task of continuous verification [Niinuma et al. 2010]. Another urgent investigation related to the practical adoption of eye movement biometrics regards the reliability of the extracted features under user physical and behavioral changes (as well as of his or her cooperation). Previous research shows that some eye movement characteristics can be influenced by several conditions, such as user fatigue [Abdulin and Komogortsev 2015], anxiety [Miltner et al. 2004], and intoxication [Nawrot et al. 2004]. Also, the results of preliminary research show that the recording time intervals can induce template aging effects, which can also affect biometric performance [Komogortsev et al. 2014a]. A comprehensive exploration of such limitations and practical considerations is very important for the future adoption

of eye movement biometrics since it would allow for the discovery of those features that can provide the optimal operational conditions in a real-world biometric scenario.

6. CONCLUSION

In this work, we utilized the saccadic eye movements of more than 300 individuals for the extraction of saccadic vigor and acceleration features, and then we incorporated the extracted features into an eye movement-driven biometric framework. Our findings support that the incorporation of the proposed features can lead to an increase in biometric accuracy and improve robustness when using different types of visual stimulus. In the future, we plan to investigate additional schemes for modeling eye movement features based on findings related to the physiological connections between eye movements and brain functionality. Also, it should be noted that the current work explored only saccadic and fixational features of eye movements, even in the case when smooth pursuit movements were exhibited in response to video stimulus. In future research, we intend to explore the properties of smooth pursuit movements to improve the accuracy and robustness of the ocular biometrics framework.

REFERENCES

E. Abdulin and O. Komogortsev. 2015. User eye fatigue detection via eye movement behavior. In *Proceedings of the 33rd Annual ACM Conference Extended Abstracts on Human Factors in Computing Systems* (2015). ACM, 1265–1270.

R. A. Abrams, D. E. Meyer, and S. Kornblum. 1989. Speed and accuracy of saccadic eye movements: Characteristics of impulse variability in the oculomotor system. *Journal of Experimental Psychology: Human Perception and Performance* 15, 529–543.

A. T. Bahill, M. R. Clark, and L. Stark. 1975. The main sequence, a tool for studying human eye movements. *Mathematical Biosciences* 24, 191–204.

A. T. Bahill and J. D. Mcdonald. 1983. Frequency limitations and optimal step size for the two-point central difference derivative algorithm with applications to human eye movement data. *IEEE Transactions on Biomedical Engineering BME-30*, 191–194.

A. T. Bahill and L. Stark. 1975. Neurological control of horizontal and vertical components of oblique saccadic eye movements. *Mathematical Biosciences* 27, 287–298.

T. A. Bahill, A. Brockenbrough, and B. T. Troost. 1981. Variability and development of a normative data base for saccadic eye movements. *Investigative Ophthalmology and Visual Science* 21, 116–125.

R. W. Baloh, A. W. Sills, W. E. Kumley, and V. Honrubia. 1975. Quantitative measurement of saccade amplitude, duration, and velocity. *Neurology* 25, 1065–1070.

R. Bednarik, T. Kinnunen, A. Mihaila, and P. Fränti. 2005. Eye-movements as a biometric. In *Image Analysis*, H. Kalviainen, J. Parkkinen and A. Kaarna (Eds.). Springer, Berlin, 780–789.

E. Bollen, J. Bax, J. G. van Dijk, M. Koning, J. E. Bos, C. G. S. Kramer, and E. A. van der Velde. 1993. Variability of the main sequence. *Investigative Ophthalmology and Visual Science* 34, 3700–3704.

L. Breiman. 2001. Random forests. *Machine Learning* 45, 5–32.

G. T. Buswell. 1935. *How People Look at Pictures: A Study of the Psychology of Perception in Art*. University of Chicago Press, Chicago, IL.

V. Cantoni, C. Galdi, M. Nappi, M. Porta, and D. Riccio. 2015. GANT: Gaze analysis technique for human identification. *Pattern Recognition* 48, 1027–1038.

L. G. Carlton and K. M. Newell. 1988. Force variability and movement accuracy in space-time. *Journal of Experimental Psychology: Human Perception and Performance* 14, 24–36.

J. E. S. Choi, P. A. Vaswani, and R. Shadmehr. 2014. Vigor of movements and the cost of time in decision making. *Journal of Neuroscience* 34, 1212–1223.

D. X. Cifu, J. R. Wares, K. W. Hoke, P. A. Wetzel, G. Gitchel, and W. Carne. 2015. Differential eye movements in mild traumatic brain injury versus normal controls. *Journal of Head Trauma Rehabilitation* 30, 21–28.

H. Collewijn, C. J. Erkelens, and R. M. Steinman. 1988a. Binocular co-ordination of human horizontal saccadic eye movements. *Journal of Physiology* 404, 157–182.

H. Collewijn, C. J. Erkelens, and R. M. Steinman. 1988b. Binocular co-ordination of human vertical saccadic eye movements. *Journal of Physiology* 404, 183–197.

T. Collins and K. Doré-Mazars. 2006. Eye movement signals influence perception: Evidence from the adaptation of reactive and volitional saccades. *Vision Research* 46, 3659–3673.

T. Collins, A. Semroud, E. Orriols, and K. Doré-Mazars. 2008. Saccade dynamics before, during, and after saccadic adaptation in humans. *Investigative Ophthalmology and Visual Science* 49, 604–612.

L. L. di Stasi, A. Antolí, and J. J. Cañas. 2011. Main sequence: An index for detecting mental workload variation in complex tasks. *Applied Ergonomics* 42, 807–813.

M. P. Eckstein, B. R. Beutter, B. T. Pham, S. S. Shimozaki, and L. S. Stone. 2007. Similar neural representations of the target for saccades and perception during search. *Journal of Neuroscience* 27, 1266–1270.

EYELINK EyeLink 1000 Eye Tracker.

T. Fawcett. 2006. An introduction to ROC analysis. *Pattern Recognition Letters* 27, 861–874.

S. J. Fricker. 1971. Dynamic measurements of horizontal eye motion. I. Acceleration and velocity matrices. *Investigative Ophthalmology* 10, 724–732.

GOOGLE Google Glass.

A. M. Haith, T. R. Reppert, and R. Shadmehr. 2012. Evidence for hyperbolic temporal discounting of reward in control of movements. *Journal of Neuroscience* 32, 11727–11736.

J. H. Holcomb, H. H. Holcomb, and A. de la Pena. 1977. Selective attention and eye movements while viewing reversible figures. *Perceptual and Motor Skills* 44, 639–644.

C. D. Holland and O. V. Komogortsev. 2013a. Complex eye movement pattern biometrics: The effects of environment and stimulus. *IEEE Transactions on Information Forensics and Security* 8, 2115–2126.

C. D. Holland and O. V. Komogortsev. 2013b. Complex eye movement pattern biometrics: Analyzing fixations and saccades. In *Proceedings of the 2013 International Conference on Biometrics (ICB)*, 1–8.

T. Ikeda and O. Hikosaka. 2007. Positive and negative modulation of motor response in primate superior colliculus by reward expectation. *Journal of Neurophysiology* 98, 3163–3170.

E. Javal. 1878. Essai sur la physiologie de la lecture. *Annales d'Oculistique* (79), 97–117, (80), 135–147, 240–274.

M. A. Just and P. A. Carpenter. 1980. A theory of reading: From eye fixations to comprehension. *Psychological Review* 87, 329–354.

P. Kasprowski and J. Ober. 2004. Eye movements in biometrics. In *Biometric Authentication*, D. Maltoni and A. K. Jain (Eds.). Springer, Berlin, 248–258.

T. Kinnunen, F. Sedlak, and R. Bednarik. 2010. Towards task-independent person authentication using eye movement signals. In *Proceedings of the 2010 Symposium on Eye-Tracking Research & Applications*. ACM, 187–190.

O. Komogortsev, C. Holland, A. Karpov, and L. R. Price. 2014b. Biometrics via oculomotor plant characteristics: impact of parameters in oculomotor plant model. *ACM Transactions on Applied Perception* 11, 1–17.

O. V. Komogortsev and C. D. Holland. 2014. The application of eye movement biometrics in the automated detection of mild traumatic brain injury. In *Proceedings of the 32nd Annual ACM Conference on Human Factors in Computing Systems (*2014). ACM, 1711–1716.

O. V. Komogortsev, C. D. Holland, and A. Karpov. 2014a. Template aging in eye movement-driven biometrics. In *SPIE, Biometric and Surveillance Technology for Human and Activity Identification XI*, 90750A–90750A–90759.

O. V. Komogortsev, A. Karpov, and C. D. Holland. 2015. Attack of mechanical replicas: Liveness detection with eye movements. *IEEE Transactions on Information Forensics and Security* 10, 716–725.

O. V. Komogortsev, A. Karpov, C. D. Holland, and H. P. Proenca. 2012b. Multimodal ocular biometrics approach: A feasibility study. In *IEEE 5th International Conference on Biometrics: Theory, Applications and Systems (BTAS)*, 209–216.

O. V. Komogortsev, A. Karpov, L. R. Price, and C. Aragon. 2012a. Biometric authentication via oculomotor plant characteristics. In *Proceedings of the 5th IAPR International Conference on Biometrics (ICB)*, 413–420.

E. Kowler, E. Anderson, B. Dosher, and E. Blaser. 1995. The role of attention in the programming of saccades. *Vision Research* 35, 1897–1916.

R. J. Leigh and D. S. Zee. 2006. *The Neurology of Eye Movements*. Oxford University Press.

S. Marcel, M. S. Nixon, and S. Z. Li. 2014. *Handbook of Biometric Anti-Spoofing: Trusted Biometrics under Spoofing Attacks*. Springer.

W. H. R. Miltner, S. Krieschel, H. Hecht, R. Trippe, and T. Weiss. 2004. Eye movements and behavioral responses to threatening and nonthreatening stimuli during visual search in phobic and nonphobic subjects. *Emotion* 4, 323–339.

K. Nandakumar, C. Yi, S. C. Dass, and A. K. Jain. 2008. Likelihood ratio-based biometric score fusion. *IEEE Transactions on Pattern Analysis and Machine Intelligence* 30, 342–347.

M. Nawrot, B. Nordenstrom, and A. Olson. 2004. Disruption of eye movements by ethanol intoxication affects perception of depth from motion parallax. *Psychological Science* 15, 858–865.

K. Niinuma, P. Unsang, and A. K. Jain. 2010. Soft biometric traits for continuous user authentication. *IEEE Transactions on Information Forensics and Security* 5, 771–780.

D. Noton and L. Stark. 1971a. Scanpaths in eye movements during pattern perception. *Science (New York, N.Y.)* 171, 308–311.

D. Noton and L. Stark. 1971b. Scanpaths in saccadic eye movements while viewing and recognizing patterns. *Vision Research* 11, 929–932.

I. Rigas, E. Abdulin, and O. Komogortsev. 2015. Towards a multi-source fusion approach for eye movement-driven recognition. *Information Fusion*, Available online: 20 August 2015.

I. Rigas, G. Economou, and S. Fotopoulos. 2012a. Biometric identification based on the eye movements and graph matching techniques. *Pattern Recognition Letters* 33, 786–792.

I. Rigas, G. Economou, and S. Fotopoulos. 2012b. Human eye movements as a trait for biometrical identification. In *IEEE 5th International Conference on Biometrics: Theory, Applications and Systems (BTAS)*, 217–222.

I. Rigas and O. V. Komogortsev. 2014. Biometric recognition via probabilistic spatial projection of eye movement trajectories in dynamic visual environments. *IEEE Transactions on Information Forensics and Security* 9, 1743–1754.

D. A. Robinson. 1964. The mechanics of human saccadic eye movement. *Journal of Physiology* 174, 245–264.

D. D. Salvucci and J. H. Goldberg. 2000. Identifying fixations and saccades in eye-tracking protocols. In *Proceedings of the 2000 Symposium on Eye Tracking Research & Applications (ETRA)*. ACM, 71–78.

B. S. Schnitzer and E. Kowler. 2006. Eye movements during multiple readings of the same text. *Vision Research* 46, 1611–1632.

A. C. Schutz, D. I. Braun, and K. R. Gegenfurtner. 2011. Eye movements and perception: A selective review. *Journal of Vision* 11, pii: 9.

R. Shadmehr, J. J. Orban de Xivry, M. Xu-Wilson, and T.-Y. Shih. 2010. Temporal discounting of reward and the cost of time in motor control. *Journal of Neuroscience* 30, 10507–10516.

SMI 2015. RED250-RED500. Retrieved from http://www.smivision.com/en/gaze-and-eye-tracking-systems/products/red-red250-red-500.html.

R. Snelick, U. Uludag, A. Mink, M. Indovina, and A. Jain. 2005. Large-scale evaluation of multimodal biometric authentication using state-of-the-art systems. *IEEE Transactions on Pattern Analysis and Machine Intelligence (PAMI)* 27, 450–455.

THEEYETRIBE. 2015. Eye Tribe Tracker. Retrieved from https://theeyetribe.com/.

J. G. Thomas. 1969. The dynamics of small saccadic eye movements. *Journal of Physiology* 200, 109–127.

TOBII. 2015. Glasses 2, http://www.tobii.com/en/eye-tracking-research/global/landingpages/tobii-glasses-2/.

R. J. van Beers. 2007. The sources of variability in saccadic eye movements. *Journal of Neuroscience* 27, 8757–8770.

A. L. Yarbus. 1967. *Eye Movements and Vision*. Plenum, New York.

J. Yingying, P. Yong, L. Bao-Liang, C. Xiaoping, C. Shanguang, and W. Chunhui. 2014. Recognizing slow eye movement for driver fatigue detection with machine learning approach. In *Proceedings of the 2014 International Joint Conference on Neural Networks (IJCNN)*, 4035–4041.

H.-J. Yoon, T. R. Carmichael, and G. Tourassi. 2014. Gaze as a biometric. In *SPIE*, 903707-903707-903707.

Y. Zhang and M. Juhola. 2012. On biometric verification of a user by means of eye movement data mining. In *Proceedings of the 2nd International Conference on Advances in Information Mining and Management (IMMM 2012)*, 85–90.

B. L. Zuber, L. Stark, and G. Cook. 1965. Microsaccades and the velocity-amplitude relationship for saccadic eye movements. *Science* 150, 1459–1460.

Received June 2015; revised October 2015; accepted October 2015